## Study of the diagonal ridges in metallicity for different star populations

Author: Pau Ubach Raya, pubachra7@alumnes.ub.edu Facultat de Física, Universitat de Barcelona, Diagonal 645, 08028 Barcelona, Spain.

Advisor: Maria Teresa Antoja Castelltort, tantoja@fqa.ub.edu

**Abstract:** Various surveys, like Gaia, GALAH and LAMOST, have uncovered many features of the Milky Way. In particular, they have uncovered diagonal ridges in metallicity in the  $(R, V_{\phi})$  plane. In this thesis, we use a realistic N-body simulation to study these ridges. We calculate the metallicity residuals for different age populations and azimuth sectors. We find that residuals decrease with age and change with azimuth. Finally, we calculate the angular momenta of the resonances of the bar and spiral arms, and we find that there is a relation between the residuals and the resonances, but it is not conclusive.

**Keywords:** Astrophysics, Galactic dynamics, Diagonal ridges, Metallicity, Radial migration **SDGs:** Quality education

### I. INTRODUCTION

#### A. Galaxies

The nature and composition of galaxies has been a subject of research for many decades. To this day, some galactic features and structures remain unexplained.

The Milky Way (MW) is a barred galaxy with spiral arms. It has several satellite galaxies, like the Sagittarius dwarf galaxy (Sgr). Various surveys, like *Gaia*, GALAH, LAMOST and APOGEE have used space and Earthbased telescopes to uncover many secrets of our galaxy.

## B. Galactic dynamics

In this subsection, we give a brief review of galactic dynamics, which is the science that studies the motion of stars, gas and dark matter (DM) in a galaxy and the causes of this motion. An extensive treatise is given by Binney and Tremaine [5].

In a galaxy, stars, gas and DM are often modelled as particles moving in a gravitational field. The position of each particle can be expressed in galactocentric Cartesian coordinates x,y,z or in galactocentric cylindrical coordinates, which are the radius R, the azimuth  $\phi$  and the vertical coordinate z. The corresponding velocity components are the radial velocity  $V_R = \dot{R}$ , the azimuthal velocity  $V_\phi = R\dot{\phi}$  and the vertical velocity  $V_z = \dot{z}$ .

An axisymmetric potential is a potential that depends only on R and z, where z is the axis of symmetry. In an axisymmetric potential, the z component of the angular momentum per unit mass,  $L_z = RV_{\phi}$ , is constant. Nearly circular orbits are approximately epicyclic and the particles that follow these orbits oscillate radially with a frequency  $\kappa$ , called epicyclic frequency.

Most patterns in disc galaxies, like bars and spiral arms, correspond to planar non-axisymmetric potentials that rotate with a constant angular speed  $\Omega_{\rm p}$ , called pattern speed. In this type of potential, particles follow epicyclic orbits with an angular speed  $\Omega$ . Particles follow closed orbits when  $\Omega - \Omega_{\rm p} = (m/n) \, \kappa$ , where m and n are integers. These particles are said to be in resonance with the pattern. The corotation resonance (CR) takes place when the particle rotates at the same speed as the pattern, that is, when  $\Omega = \Omega_{\rm p}$ . The inner Lindblad resonance (ILR) occurs when  $\Omega = \Omega_{\rm p} + \kappa/2$  and the outer Lindblad resonance (OLR) occurs when  $\Omega = \Omega_{\rm p} - \kappa/2$ .

Action variables are canonical coordinates that are adiabatic invariants. In a non-axisymmetric potential, the axisymmetric action estimates  $J_R, J_\phi, J_z$  are used as action variables, although they are not strictly constant.  $J_R$  is a measure of orbit eccentricity,  $J_z$  is a measure of orbit inclination and  $J_\phi$  is equal to  $L_z$ .

#### C. Diagonal ridges

Analyzing Gaia DR2, Antoja et al. [1] and Kawata et al. [20] observed substructures in stellar number density in the  $(R, V_{\phi})$  plane, called diagonal ridges. Antoja et al. [2] also observed diagonal ridges in Gaia DR3. The origin of these ridges is still not clear, but several mechanisms have been proposed to explain it.

Some ridges could be linked to resonances of the bar. Using an N-body simulation, Fragkoudi et al. [9] demonstrated that the longest and most prominent ridge in the simulation is associated with the OLR of the bar. Monari et al. [31] showed that a model with a slowly rotating large bar can create ridges associated with several resonances. A similar result was obtained by Asano et al. [3] with an N-body simulation of a MW-like galaxy, and by Laporte et al. [24], who studied the ridges for young and old stellar populations.

Ridges can appear due to resonances of density-wave spiral arms. Michtchenko et al. [27, 28] showed that a model with bar and spiral arms can generate a ridge related to the CR of the spiral arms and ridges related to high-order resonances around it. Barros et al. [4] arrived at the same result using a model with spiral arms alone.

Another mechanism that causes ridges is the phase mixing induced by transient spiral structure. Hunt et al. [17, 18] demostrated that a long slow bar or a short fast bar combined with transient winding spiral arms creates ridges that are qualitatively consistent with *Gaia* DR2. Khanna et al. [21] used a toy model with four spiral arms that also produces ridges. Martinez-Medina et al. [25] showed that the ridges of a simulation with a bar and spiral arms correlate with wiggles in the rotation curve.

Perturbations of a satellite galaxy can also give rise to ridges. Laporte et al. [23] analyzed the interaction between a MW-like galaxy and a Sgr-like perturber using an N-body simulation and showed that ridges are present. Khanna et al. [21] studied two perturbers with different masses. Antoja et al. [2] examined several models of tidally induced spiral arms, and compared them to Gaia DR3.

## D. Diagonal ridges in chemical properties

The diagonal ridge substructures in the  $(R, V_{\phi})$  plane can also be seen in several chemical properties, like the iron abundance [Fe/H] and the alpha abundance [ $\alpha$ /Fe]. Analyzing GALAH DR2, Khanna et al. [21] observed ridges in [Fe/H] and [ $\alpha$ /Fe] with a sharp change in [Fe/H]. They found that ridges are comprised of metalrich and alpha-poor stars, that is, young stars. Using a model, Fragkoudi et al. [10] found that all ridges have younger stars. Wang et al. [34] and Yang et al. [36] observed ridges in LAMOST data for all age populations. Wheeler et al. [35] explored the chemical signatures of bar resonances. Haywood et al. [16] studied the slowdown of a bar using metallicity gradients.

# E. Thesis

There are not many papers that thoroughly study the relation between the metallicity and the kinematic ridges. In this thesis, we use a full N-body simulation to study this relation and its connection with resonances.

In section II-A, we describe the N-body simulation that we study. In section II-B, we analyze the metallicity gradient and the diagonal ridges in metallicity for different age groups. In section II-C, we represent the metallicity residuals as a function of  $L_z$  for different azimuths and ages. In section II-D, we find the resonances and explore the relation between the residuals and the resonances. Finally, we conclude in section III.

#### II. DEVELOPING SECTIONS

## A. N-body simulation

We study the model M1\_c\_b that was first described by Fiteni et al. [8] and further explained by Ghosh, Debattista and Khachaturyants [13]. This is an N-body + smooth particle hydrodynamics simulation. Initially, it consists of a gas corona in pressure equilibrium with a dark matter halo. It evolves for 13 Gyr, forming a large-scale bar. Stars form out of cooling gas. The simulation has 2600 snapshots, with a time interval of 5 Myr per snapshot. We study the snapshots 1700 (8.5 Gyr) and 2600 (13 Gyr) using the Python packages numpy, scipy, matplotlib and pynbody.

First, we analyze the snapshot 1700. Figure 1 shows the stellar number density in the (x,y) plane. This is the face-on view of the galaxy. Figure 2 shows the stellar number density in the  $(R,V_\phi)$  plane. In this figure, we can see the diagonal ridges in density, which are similar to those observed by Gaia.

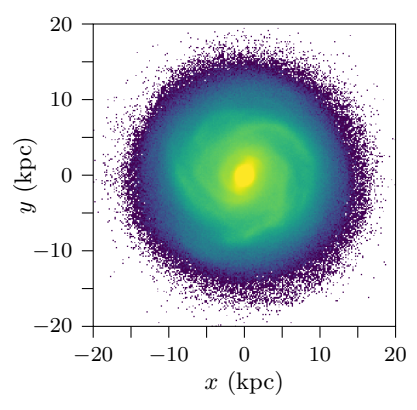


FIG. 1: 2D histogram of the stars in the (x,y) plane for the snapshot 1700. The bin lengths are  $\Delta x = \Delta y = 0.16$  kpc. The scale of the colormap is logarithmic.

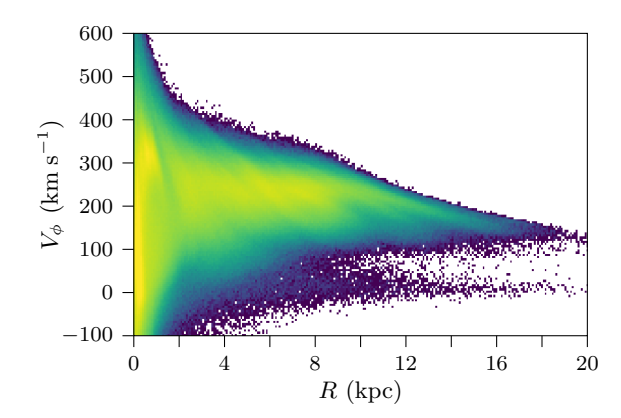


FIG. 2: 2D histogram of the stars in the  $(R, V_{\phi})$  plane for the snapshot 1700. The bin lengths are  $\Delta R = 0.08$  kpc and  $\Delta V_{\phi} = 5$  km s<sup>-1</sup>. The scale of the colormap is logarithmic.

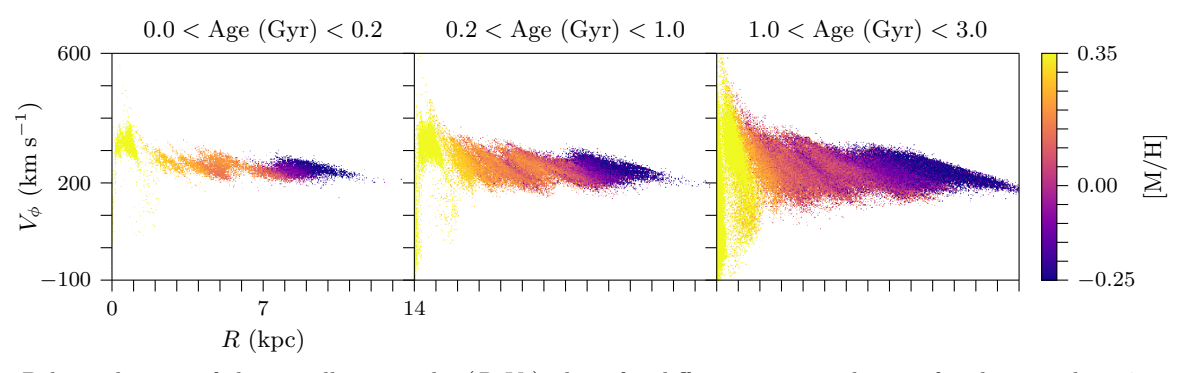


FIG. 3: 2D binned mean of the metallicity in the  $(R, V_{\phi})$  plane for different age populations for the snapshot 1700. The bin lengths are  $\Delta R = 0.04$  kpc and  $\Delta V_{\phi} = 2.5$  km s<sup>-1</sup>. The colormap is linear and it is saturated at -0.25 and 0.35 to highlight the diagonal ridges in metallicity.

## B. Diagonal ridges in metallicity

The most common way to represent the metallicity is the iron abundance [Fe/H]. However, we use the total metallicity [M/H], which is the abundace of heavy elements (metals) with respect to the Sun.

For the snapshot 1700, Figure 3 shows three plots of the mean metallicity in the  $(R, V_{\phi})$  plane, each one corresponding to a different age group. In all age groups, metallicity decreases with radius, that is, the radial metallicity gradient is negative. This trend occurs in most disc galaxies and it can be caused by an inside-out disc growth, where stars in the inner regions form earlier than stars in the outer regions, enriching the inner regions earlier [26]. It can also be due to an equilibrium scenario, where the metallicity at each radius rapidly evolves toward an equilibrium state [19].

Both the inside-out growth and the equilibrium scenario predict a monotonic decrease in metallicity with radius. However, in Figure 3 we can see local increases and decreases of metallicity in the form of diagonal ridges. These diagonal ridges in metallicity might be caused by radial migration, which is the motion of stars from one radius to another. More specifically, ridges might appear because non-axisymmetric forces change the angular momenta of the stars and they become trapped at a resonance, like the CR of transient spiral arms [33], the resonance overlap of a bar and spiral arms [29, 30] or the resonances of a bar that is slowing down [14, 22]. This process of radial migration is called churning.

The global structure of the ridges does not change for different age populations. Each ridge approximately follows the same line of constant  $L_z$ , which is a reciprocal function of the form  $V_{\phi} = L_z/R$ . This happens because stars become trapped at the resonance related to the ridge, where the angular momentum does not change.

The eccentricity of the orbits becomes greater as stars get older, that is, the radial action  $J_R$  increases with age. This process of radial migration is called blurring [32, 33].

It is the reason why the velocity dispersion increases with age.

### C. Metallicity residuals

To study the variations of metallicity with age and azimuth, we calculate the differences (residuals) between the mean metallicity of an azimuth sector and the mean metallicity of the whole disc (all azimuths). In Figure 4, we represent the residuals as a function of  $L_z$ . We choose  $L_z$  in favor of R because the diagonal ridges in metallicity follow lines of approximately constant  $L_z$ , and  $L_z$  is an adiabatic invariant that can be simply calculated with R and  $V_\phi$  without assuming any potential.

In the top panel of Figure 4, we represent the residuals of the snapshot 1700 for the azimuth sector  $0 < \phi <$  $\pi/4$  and several age populations. We can see that the absolute value of the residuals decreases with age. This occurs because blurring flattens the radial metallicity gradient and the deviations from it over time, blurring out the diagonal ridges in metallicity. For the age populations (0,0.2), (0.2,1), (1,3) and (3,6) Gyr, the extreme values of the residuals are 0.11, 0.10, 0.06 and 0.03 dex, respectively. These values are consistent with those of Wheeler et al. [35], who represented  $J_{\phi}$ -[Fe/H] at different  $J_R$  using a simulation and found that the residuals are  $\sim 0.1$  dex. Despite the consistency of the results, we cannot compare them because their test particle simulation is less realistic than our N-body simulation.

In the middle panel of Figure 4, we represent the residuals of the snapshot 1700 for the age population 0.0 Gyr < Age < 0.2 Gyr and several azimuth sectors, shown in several colors. We have chosen one half of the galaxy since the dominant mode is m=2. We can see that the residuals change with azimuth. These azimuthal metallicity variations are produced because stars follow "banana-shaped" orbits that change with azimuth [35]. For the azimuth sectors  $(0, \pi/4)$ ,  $(\pi/4, \pi/2)$ ,  $(\pi/2, 3\pi/4)$  and  $(3\pi/4, \pi)$ , the extreme values of the residuals are

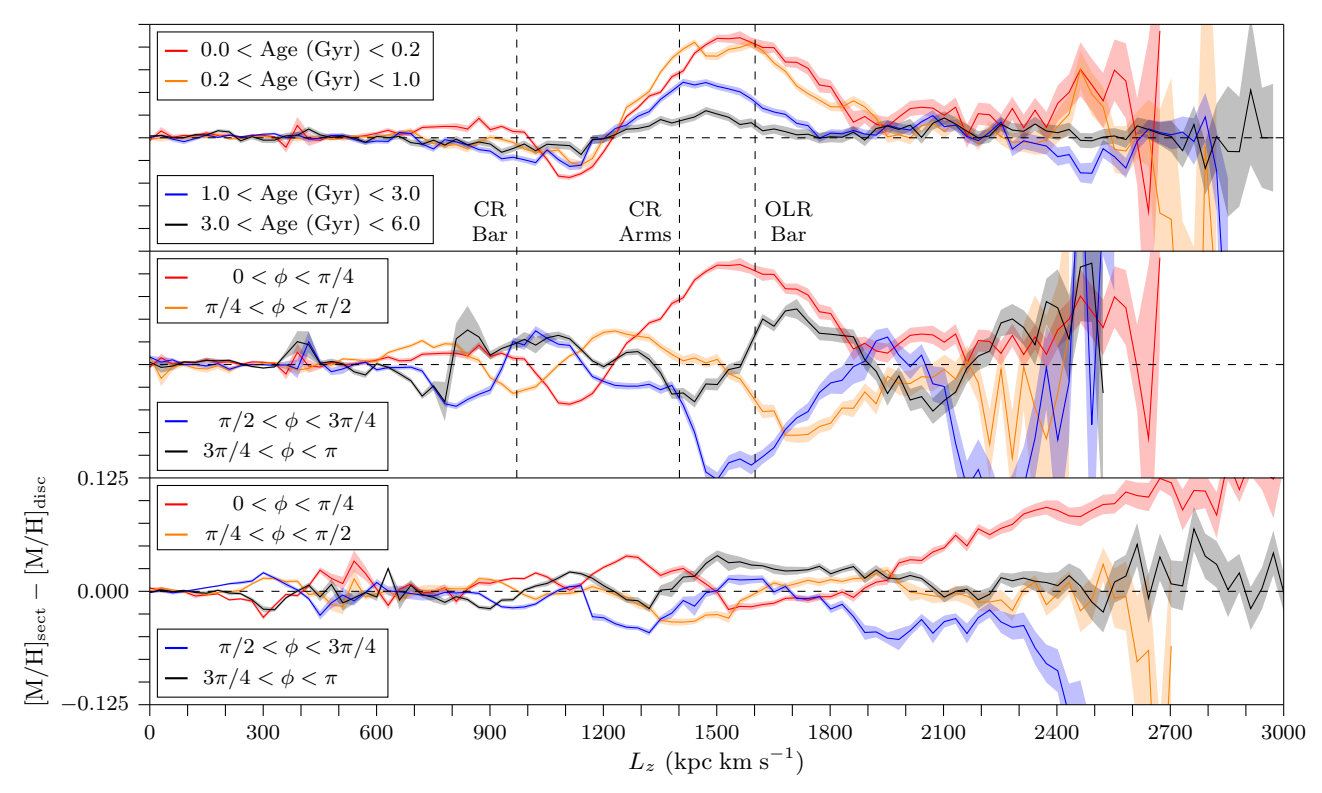


FIG. 4: Residuals between the mean metallicity of an azimuth sector and the mean metallicity of the whole disc (all azimuths) as a function of  $L_z$ . The bin length is 30 kpc km s<sup>-1</sup>. The shaded areas represent the propagated error of the standard errors of the mean. The most significant resonances of the snapshot 1700 are indicated with vertical dashed lines. *Top*: snapshot 1700: the plots correspond to the azimuth sector  $0 < \phi < \pi/4$  and several age populations, shown in different colors. *Middle*: snapshot 1700: the plots correspond to the age population 0.0 < Age (Gyr) < 0.2 and several azimuth sectors, shown in different colors. *Bottom*: the same as the middle, but for the snapshot 2600.

0.11, -0.08, -0.12 and 0.06 dex, respectively. These values are of the same order as the observations of the MW made by Hawkins [15], who studied two samples from LAMOST and Gaia DR3 and found that the average metallicity variations at fixed radius can be as high as  $\sim 0.10$  dex. The changes in azimuth are compatible with the scales of variations of the spiral arms.

For each bin in Figure 4, we calculate the standard deviation of the metallicities and the corresponding standard errors of the mean (SEMs). By calculating the quadratic sum of the SEMs, we obtain the error of each residual.

In the top and the middle panels of Figure 4, the residuals and the error experience great variations for high values of  $L_z$ . This erratic behaviour occurs because at high values of  $L_z$  there is a lack of stars.

The bottom panel of Figure 4 shows the same as the middle panel, but for the snapshot 2600. In this case, the absolute value of the residuals is lower than the case of the snapshot 1700 due to blurring. In this case, the erratic behaviour of the residuals at high  $L_z$  is less noticable because stars have spread over time.

## D. Residuals and resonances

Using the power spectra given by Debattista et al [7], we calculate the pattern speeds and the resonances of the bar and the spiral arms. We take the m=2 Fourier component, which corresponds to a two-armed structure. The power maximum above 49 km s<sup>-1</sup> kpc<sup>-1</sup> corresponds to the pattern speed of the bar and the power maxima below 49 km s<sup>-1</sup> kpc<sup>-1</sup> correspond to the pattern speeds of the spiral arms. The intersection between  $\Omega_{\rm p}$  and the curve  $\Omega$  gives the radius of the CR. The intersections between  $\Omega_{\rm p}$  and the curves  $\Omega \pm \kappa/2$  give the radii of the OLR and the ILR. To obtain the angular momentum  $L_z$  of a resonance, we multiply  $\Omega$  by the square of the radius of the resonance.

In the snapshot 1700, there is a bar with a pattern speed  $\Omega_{\rm p}=64.6~{\rm km~s^{-1}~kpc^{-1}}$  and there are inner spiral arms with  $\Omega_{\rm p}=43.0~{\rm km~s^{-1}~kpc^{-1}}$ . The CR of the bar lies at  $L_z=970~{\rm kpc~km~s^{-1}}$ , the OLR of the bar is located at  $L_z=1600~{\rm kpc~km~s^{-1}}$  and the CR of the spiral arms is situated at  $L_z=1400~{\rm kpc~km~s^{-1}}$ . These resonances are shown in the top and middle panels of Figure 4.

In the snapshot 2600, there is almost no bar. There are inner spiral arms, with the ILR at  $L_z = 680 \text{ kpc km s}^{-1}$ ,

the CR at  $L_z=1590~\rm kpc~km~s^{-1}$  and the OLR at  $L_z=2590~\rm kpc~km~s^{-1}$ . However, since they seem to have no clear correspondence with residuals, we do not include them in Figure 4.

The CR of the spiral arms and the OLR of the bar form a resonance overlap. Our hypohesis is that there is a relation between the residuals and some resonances of the bar and spiral arms. Representing the top panel of Figure 4 for several azimuth sectors other than  $0 < \phi < \pi/4$ , we see that there is sometimes a metallicity peak at the CR of the bar and there are sometimes peaks around it. Furthermore, we see that there are peaks at the resonance overlap or around it.

These metallicity peaks are somewhat consistent with the features found by Wheeler et al. [35], who found a wave-crest at the OLR of the bar, and Haywood et al. [16], who found an accumulation of metal-rich star up to the OLR.

## III. CONCLUSIONS

We use an N-body simulation to study the diagonal ridges in metallicity for several star populations. We calculate the residuals between the mean metallicity of an azimuth sector and the mean metallicity of the whole disc (all azimuths) as a function of  $L_z$ . We plot the residuals for two snapshots, for several age populations and for several azimuth sectors. We find that:

- The absolute value of the residuals decreases with age. This is caused by blurring.
- The residuals change with azimuth. The azimuthal

metallicity variations are produced because the "banana-shaped" orbits that stars follow change with azimuth.

Finally, we calculate the angular momenta of the resonances of the bar and the spiral arms. We see that there are some metallicity peaks at some of the resonances or around them. We hypothesize that there is a connection between the residuals and the resonances, but our results are not conclusive and this topic needs to be further studied.

When we study the ridges for several azimuth sectors, we choose one half of the galaxy. In future work, it could be interesting to explore the level of asymmetries in the galaxy. It would also be interesting to use the angle variables instead of the real azimuth because we would be able to better understand what is happening at a theoretical level.

Future surveys and data releases, like *Gaia* DR4, WEAVE, and 4MOST will provide data for larger samples and larger distances. The results of this thesis might serve as a prediction for these future observations.

## Acknowledgments

I want to thank my advisor, Teresa Antoja, for her invaluable help and guidance. I would also like to thank Karl Fiteni and Victor Debattista for their simulation, Judith Ardèvol for helping me with Topcat and Testuro Asano for his simulation.

Last but not least, I want to thank my parents and my sister for their love and support.

- [1] T. Antoja et al., Nature **561**, 360 (2018).
- [2] T. Antoja et al., A&A 668, A61 (2022).
- [3] T. Asano et al., MNRAS **499**, 2416 (2020).
- [4] D. A. Barros et al., ApJ 888, 75 (2020).
- [5] J. Binney and S. Tremaine. *Galactic dynamics*. 2nd ed. Princeton: Princeton University Press, 2008.
- [6] V. P. Debattista et al., MNRAS 469, 1587 (2017).
- [7] V. P. Debattista et al., MNRAS **537**, 1620 (2025).
- [8] K. Fiteni et al., MNRAS 503, 1418 (2021).
- [9] F. Fragkoudi et al., MNRAS 488, 3324 (2019).
- [10] F. Fragkoudi et al., MNRAS **494**, 5936 (2020).
- [11] Gaia Collaboration, A&A 616, A1 (2018).
- [12] Gaia Collaboration, A&A **616**, A11 (2018).
- [13] S. Ghosh, V. P. Debattista and T. Khachaturyants, MNRAS 511, 784 (2022).
- [14] A. Halle et al., A&A 578, A58 (2015).
- [15] K. Hawkins, MNRAS 525, 3318 (2023).
- [16] M. Haywood et al., A&A **690**, A147 (2024).
- [17] J. A. S. Hunt et al., MNRAS **481**, 3794 (2018).
- [18] J. A. S. Hunt et al., MNRAS 490, 1026 (2019).
- [19] J. W. Johnson et al., preprint, arXiv:2410.13256 (2024).

- [20] D. Kawata et al., MNRAS 479, L108 (2018).
- [21] S. Khanna et al., MNRAS 489, 4962 (2019).
- [22] S. Khoperskov et al., A&A 638, A144 (2020)
- [23] C. F. P. Laporte et al., MNRAS 485, 3134 (2019).
- [24] C. F. P. Laporte et al., A&A **643**, L3 (2020).
- [25] L. Martinez-Medina et al., MNRAS 485, L104 (2019).
- [26] F. Matteucci and P. François, MNRAS 239, 885 (1989).
- [27] T. A. Michtchenko et al., A&A 615, A10 (2018).
- [28] T. A. Michtchenko et al., ApJL 863, L37 (2018).
- [29] I. Minchev and B. Famaey, ApJ 722, 112 (2010).
- [30] I. Minchev et al., A&A **527**, A147 (2011).
- [31] G. Monari et al., A&A **626**, A41 (2019).
- [32] R. Schönrich and J. Binney, MNRAS **396**, 203 (2009).
- [33] J. A. Sellwood and J. J. Binney, MNRAS **336**, 785 (2002).
- [34] H.-F. Wang et al., ApJ 902, 70 (2020).
- [35] A. Wheeler et al., ApJ **935**, 28 (2022).
- [36] P. Yang et al., AJ **165**, 110 (2023.)

## Estudi de les crestes diagonals en metal·licitat per a diferents poblacions estel·lars

Author: Pau Ubach Raya, pubachra7@alumnes.ub.edu Facultat de Física, Universitat de Barcelona, Diagonal 645, 08028 Barcelona, Spain.

Advisor: Maria Teresa Antoja Castelltort, tantoja@fqa.ub.edu

**Resum:** Diversos rastrejos, com Gaia, GALAH and LAMOST, han descobert moltes característiques de la Via Làctia. En particular, han descobert crestes diagonals en metal·licitat al pla  $(R, V_{\phi})$ . En aquest treball, utilitzem una simulació de N cossos realista per estudiar aquestes crestes. Calculem els residuals de metal·licitat per a diferents poblacions d'edat i sectors azimutals. Trobem que els residuals decreixen amb l'edat i canvien amb l'azimut. Finalment, calculem els moments angulars de les ressonàncies de la barra i dels braços espirals, i trobem que hi ha una relació entre els residuals i les ressonàncies, però no és concloent.

Paraules clau: Astrofísica, Dinàmica galàctica, Crestes diagonals, Metal·licitat, Migració radial ODSs: Educació de qualitat.

## Objectius de Desenvolupament Sostenible (ODSs o SDGs)

1. Fi de la es desigualtats		10. Reducció de les desigualtats
2. Fam zero		11. Ciutats i comunitats sostenibles
3. Salut i benestar		12. Consum i producció responsables
4. Educació de qualitat	Х	13. Acció climàtica
5. Igualtat de gènere		14. Vida submarina
6. Aigua neta i sanejament		15. Vida terrestre
7. Energia neta i sostenible		16. Pau, justícia i institucions sòlides
8. Treball digne i creixement econòmic		17. Aliança pels objectius
9. Indústria, innovació, infraestructures		

Treball de Fi de Grau 6 Barcelona, June 2025